CMS Physics Analysis Summary

Contact: cms-pag-conveners-heavyions@cern.ch 2012/08/13

Prompt and non-prompt J/ψ R_{AA} with 150 μb^{-1} integrated PbPb luminosity at $\sqrt{s_{NN}}$ = 2.76 TeV

The CMS Collaboration

Abstract

This document presents updated results on the $J/\psi \to \mu^+\mu^-$ measurement in collisions at $\sqrt{s_{NN}} = 2.76$ TeV, based on a data sample collected during the 2011 PbPb run with the CMS experiment at the LHC, which corresponds to an integrated luminosity of 150 μb^{-1}. The prompt and non-prompt J/ψ contributions are separated and the yields compared to those in pp at 2.76 TeV scaled by the number of binary collisions in the form of nuclear modification factor, R_{AA}, in different bins of event centrality, and J/ψ p_T and rapidity. The high-p_T prompt J/ψ show a suppression that does not vary with rapidity, and, in the forward rapidity region, are as suppressed as the low-p_T J/ψ. Non-prompt J/ψ R_{AA} dependence with p_T and rapidity was measured in fine bins of centrality. These represent the first detailed measurements, in heavy-ion collision, of the b-quark energy loss kinematic dependence.

1 Introduction

At large energy densities and high temperatures, strongly interacting matter consists of a deconfined and chirally-symmetric system of quarks and gluons [1], often referred to as "quark-gluon plasma" (QGP) [2]. The formation of a QGP in high-energy nuclear collisions can be evidenced in a variety of ways. One of the most striking signatures is the suppression of quarkonium states [3], both of the charmonium (J/ψ, ψ(2S), χ_c, etc.) and the bottomonium (Y(1S, 2S, 3S), χ_b, etc.) families. This suppression is thought to be a direct effect of deconfinement, when the binding potential between the constituents of a quarkonium state, a heavy quark (Q) and its antiquark ($\overline{\mathrm{Q}}$), is screened by the colour charges of the surrounding light quarks and gluons. The suppression is predicted to occur above a certain dissociation temperature of the medium (T_d) depending on the $\mathrm{Q\overline{Q}}$ binding energy. Since the Y(1S) is the most tightly bound state among all quarkonia, it is expected to be the one with the highest dissociation temperature, while the ψ(2S) with the lowest binding energy, to be the one with the lowest dissociation temperature and hence the first to melt. However, there are further possible changes to the quarkonium production in heavy-ion collisions. On the one hand, cold-nuclear-matter effects, such as the modifications of the parton distribution functions inside the nucleus (shadowing), can reduce the production of quarkonia without the presence of a QGP [4, 5]. On the other hand, the large number of heavy quarks produced in heavy-ion collisions, in particular at the energies accessible by the Large Hadron Collider (LHC), could lead to an increased production of quarkonia via statistical recombination [6–11].

At LHC energies, the inclusive J/ψ yield contains a significant non-prompt contribution from b-hadron decays [12–14]. Owing to the long lifetime of the b hadrons ($\mathcal{O}(500)\,\mu\mathrm{m}/c$), compared to the QGP lifetime ($\mathcal{O}(10)\,\mathrm{fm}/c$), this contribution should not suffer from colour screening, but instead reflects the b-quark energy loss in the medium. Such energy loss would lead to a suppression of the b-hadron yield at high p_{T}. The importance of an unambiguous, detailed, measurement of open bottom flavour is driven by the lack of knowledge regarding key features of the dynamics of parton energy loss in the QGP, such as its colour-charge and parton-mass dependencies [15, 16] and the relative role of radiative and collisional energy loss [17].

Experimentally, the suppression is quantified by the ratio of the yield measured in heavy-ion collisions and a reference, which usually is the yield measured in pp collisions, the 'vacuum-like' system where no QGP is formed. Such a ratio is called the nuclear modification factor, R_{AA}. In the absence of medium effects, one would expect $R_{AA} = 1$ for hard processes, which scale with the number of inelastic nucleon-nucleon collisions. The R_{AA} of prompt and non-prompt J/ψ has been measured separately by CMS in bins of transverse momentum (p_{T}), rapidity (y) and collision centrality [18]. A strong, centrality-dependent suppression has been observed for J/ψ with $p_{\mathrm{T}} > 6.5\,\mathrm{GeV}/c$. The ALICE experiment has acceptance down to $p_{\mathrm{T}} = 0$ and has shown a moderate ($R_{AA} \simeq 0.6$) suppression of inclusive J/ψ for all centralities, at forward rapidity [19].

This document describes the updated R_{AA} measurements of prompt and non-prompt J/ψ mesons produced in PbPb collisions at $\sqrt{s_{\mathrm{NN}}} = 2.76\,\mathrm{TeV}$, using and integrated luminosity of $\mathcal{L}_{\mathrm{int}} = 150\,\mu\mathrm{b}^{-1}$. This corresponds to an increase of the PbPb data sample by a factor 20 compared to the 2010 results published previously by CMS [18]. The *non-prompt* J/ψ from B-hadron decays have been separated from *prompt* J/ψ utilizing the reconstructed decay vertex of the $\mu^+\mu^-$ pair. Directly-produced J/ψ as well as those from decays of higher charmonium states (e.g. ψ(2S) and χ_c) are considered *prompt* as their decay length is unmeasurably small compared to those from B decays and are not distinguished in this analysis. Using data from the pp run at $\sqrt{s}$ = 2.76 TeV, the R_{AA} is calculated as

$$R_{AA} = \frac{\mathcal{L}_{\mathrm{pp}}}{T_{AA} N_{\mathrm{MB}}} \frac{N_{\mathrm{PbPb}}}{N_{\mathrm{pp}}} \cdot \frac{\varepsilon_{\mathrm{pp}}}{\varepsilon_{\mathrm{PbPb}}}, \quad (1)$$

where

- N_{PbPb} is the raw number of prompt J/ψ or non-prompt J/ψ decayed in the $\mu^+\mu^-$ channel measured in PbPb;
- N_{pp} is the raw number of prompt J/ψ or non-prompt J/ψ decayed in the $\mu^+\mu^-$ channel measured in pp;
- N_{MB} is the number of minimum-bias events in PbPb sampled by the event selection and is 1.16×10^9;
- $\varepsilon_{\mathrm{pp}}$ and $\varepsilon_{\mathrm{PbPb}}$ are the combined trigger and reconstruction efficiency in pp and PbPb respectively;
- T_{AA} is the nuclear overlap function, namely the number of elementary binary nucleon-nucleon (NN) collisions divided by the elementary NN cross section. It can be interpreted as the NN-equivalent integrated luminosity per nucleus-nucleus (AA) collision for a given centrality [20]. It varies as a function of centrality of the collision and is typically given in units of mb^{-1}; and
- $\mathcal{L}_{\mathrm{pp}} = (231 \pm 14)\,\mathrm{nb}^{-1}$ is the integrated luminosity of the pp data set.

2 The CMS detector

A detailed description of the CMS detector can be found in Ref. [21]; we briefly mention here the detector subsystems used for this analysis.

Muons are detected in the pseudo-rapidity interval $|\eta| < 2.4$ by gaseous detectors made of three technologies: drift tubes, cathode strip chambers, and resistive plate chambers, embedded in the steel return yoke. The silicon tracker is composed of pixel detectors (three barrel layers and two forward disks on either side of the detector, made of 66 million $100 \times 150\,\mu\mathrm{m}^2$ pixels) followed by microstrip detectors (ten barrel layers plus three inner disks and nine forward disks on either side of the detector, with strips of pitch between 80 and 180 μm). The transverse momentum of muons matched to reconstructed tracks is measured with a resolution better than $\sim$1.5% for p_{T} smaller than 100 GeV/c [22]. The good resolution is the result of the 3.8 T magnetic field and the high granularity of the silicon tracker.

In addition, CMS has extensive forward calorimetry, including two steel/quartz-fibre Cherenkov forward hadron (HF) calorimeters, which cover $2.9 < |\eta| < 5.2$. These detectors are used in the present analysis for the event selection and PbPb collision centrality determination. Two beam scintillator counters (BSC) are installed on the inner side of the HF calorimeters for triggering and beam-halo rejection.

3 Data Selection

3.1 Event selection

Inelastic hadronic PbPb collisions are selected using information from the HF calorimeters and the BSC, in coincidence with a bunch crossing identified by the beam pick-ups, BPTX, (one on each side of the detector) [21]. Events are further filtered offline by requiring a reconstructed

primary vertex based on at least two tracks, and at least 3 towers on each HF with an energy deposit of more than 3 GeV per tower. These criteria reduce contributions from single-beam interactions with the environment (e.g. beam-gas collisions and collisions of the beam halo with the beam pipe), ultra-peripheral electromagnetic interactions, and cosmic-ray muons. A small fraction of the most peripheral PbPb collisions are not selected by these *minimum-bias* requirements that select (97$\pm$3)% of the inelastic hadronic cross section [23]. After correcting for this source of inefficiency, a sample corresponding to 1.16×10^9 minimum-bias events passes all these filters. Assuming a PbPb cross-section of 7.65 b [23], this corresponds to an integrated luminosity of $\mathcal{L}_{\rm int} \approx 150\,\mu{\rm b}^{-1}$.

The measurements reported here are based on dimuon events triggered by the Level-1 (L1) trigger, a hardware-based trigger that uses information from the muon detectors. The trigger used had no constraints on the momentum of the muons.

The centrality of heavy-ion collisions, i.e. the geometrical overlap of the incoming nuclei, is related to the energy released in the collisions. In CMS, centrality is defined as percentiles of the distribution of the energy deposited in the HFs. Using a Glauber-model calculation as described in Ref. [23], one can estimate variables related to the centrality, such as the mean number of nucleons participating in the collisions ($N_{\rm part}$), the mean number of binary nucleon-nucleon collisions ($N_{\rm coll}$) or the average nuclear overlap function (T_{AA}). The most central (highest HF energy deposit) and most peripheral (lowest HF energy deposit) centrality bins used in the analysis are 0–5% and 60–100%, and 0–10% and 50–100%, for prompt and non-prompt J/ψ results respectively. In the following, $N_{\rm part}$ will be the variable used to show the centrality dependence of the measurements, and its value, computed for events with flat centrality distribution, ranges from 381$\pm$2 in the 0-5% bin to 14$\pm$2 in the 60-100% bin. It should be noted that the most peripheral bin (60-100%) is rather wide and mostly populated by dimuon events with centrality values close to 60%. If the events would be distributed according to the number of elementary collisions, $N_{\rm coll}$, which suits well for initially-produced hard probes (for which $R_{AA} = 1$ in absence of any medium effects), the average $N_{\rm part}$ would become 25 instead of 14 for this bin. For the other finer bins, the difference is negligible (less than 3%).

Results are presented also in three bins of $|y|$ ([0,1.2], [1.2,1.6], [1.6,2.4]) and four bins in $p_{\rm T}$ ([6.5,8], [8,10], [10,13], [13,30] GeV/c). At forward rapidity, $1.6 < |y| < 2.4$, a measurement in a lower $p_{\rm T}$ interval [3,6.5] GeV/c has been performed.

The pp reference sample, at the same center of mass colliding energy, with an integrated luminosity of $\mathcal{L}_{\rm int} = (231 \pm 14)\,{\rm nb}^{-1}$, has been recorded and has been reconstructed with the same heavy-ion algorithm. This data set was triggered by a looser dimuon trigger than of the 2011 PbPb data set, in that the single muons had more relaxed quality selection criteria, while still no explicit momentum threshold was imposed.

3.2 Muon selection

The muon offline reconstruction algorithm starts by reconstructing tracks in the muon detectors. These tracks are then matched to tracks reconstructed in the silicon tracker by means of an algorithm optimized for the heavy-ion environment [24, 25]. The final muon-track parameters result from a global fit of the muon and a tracker track. Due to better momentum resolution, up to $p_{\rm T} \sim$100 GeV/c, the kinematics of the global fit are assigned to be those of the inner track. These are the muons used in this analysis.

The same single muon acceptance criteria as in Ref. [18] have been applied to ensure reasonable

($> 10\%$) reconstruction efficiencies:

$$\begin{aligned} p_{\mathrm{T}}^{\mu} &> 3.4\,\mathrm{GeV}/c && \text{for } |\eta^{\mu}| < 1.0, \\ p_{\mathrm{T}}^{\mu} &> (5.8 - 2.4 \times |\eta^{\mu}|)\,\mathrm{GeV}/c && \text{for } 1.0 < |\eta^{\mu}| < 1.5, \\ p_{\mathrm{T}}^{\mu} &> (3.4 - 0.78 \times |\eta^{\mu}|)\,\mathrm{GeV}/c && \text{for } 1.5 < |\eta^{\mu}| < 2.4. \end{aligned} \tag{2}$$

Additional muon selection criteria (number of valid tracker hits, $\chi^2/ndof$ of both the inner track and the global fit, etc) are applied as reported in the same reference.

4 Signal extraction

The identification of J/ψ mesons coming from b-hadron decays relies on the measurement of a secondary $\mu^+\mu^-$ vertex displaced from the primary collision vertex. The displacement between the $\mu^+\mu^-$ vertex and the primary vertex $\vec{r}$ is measured in the plane transverse to the beam direction. The most probable transverse b-hadron decay length in the laboratory frame [26, 27] is calculated as

$$L_{xy} = \frac{\hat{u}^T S^{-1} \vec{r}}{\hat{u}^T S^{-1} \hat{u}}, \tag{3}$$

where $\hat{u}$ is the unit vector in the direction of the J/ψ meson p_{T} and S is the sum of the primary and secondary vertex covariance matrices. From this quantity (which is the projected decay length of the J/ψ onto the transverse plane), the pseudo-proper decay length $\ell_{\mathrm{J}/\psi} = L_{xy}\, m_{\mathrm{J}/\psi} / p_{\mathrm{T}}$ is computed as an estimate of the b-hadron decay length.

To measure the fraction of non-prompt J/ψ (the b-*fraction*), the invariant-mass spectrum of $\mu^+\mu^-$ pairs and their $\ell_{\mathrm{J}/\psi}$ distribution are fitted simultaneously in an extended unbinned maximum likelihood fit, in bins of p_{T}, rapidity and event centrality. In this fit, the fraction of non-prompt J/ψ is a free parameter. Several parameters are fixed before this last fitting stage: resolution function parameters are fixed from the prompt MC template and lifetime background function parameters are fixed from fits to the data sidebands. As the dominant effect on the signal mass shape is the rapidity-dependent mass resolution, for the p_{T} and y binning, all parameters of the fit are left free. In the case of centrality binning, the sigma of the Crystal-Ball function is left free while the rest of the parameters are fixed to the minbias bin with given p_{T} and y bin.

The fitting procedure is similar to the one used in the pp analysis at $\sqrt{s}$ = 7 TeV [28] and 2010 PbPb analysis at $\sqrt{s}$ = 2.76 TeV [18]. The invariant-mass spectrum is fitted with an exponential for the background and the sum of a Crystal Ball[1] and a Gaussian function, with common mean, for the signal. The differences compared to the 2010 PbPb analysis are two: using independent widths for the two signal functions in the mass fits, and in the parametrization of the resolution function to describe $\ell_{\mathrm{J}/\psi}$. The resolution function is now comprised of the sum of two Gaussians which depend on the per-event uncertainty of the measured $\ell_{\mathrm{J}/\psi}$, determined from the covariance matrices of the primary and secondary vertex fits. One Gaussian function

[1] The Crystal Ball function is defined as:

$$f_{CB}(m) = \begin{cases} \frac{N}{\sqrt{2\pi}\sigma} \exp\left(-\frac{(m-m_0)^2}{2\sigma^2}\right), & \text{for } \frac{m-m_0}{\sigma} > -\alpha; \\ \frac{N}{\sqrt{2\pi}\sigma} \left(\frac{n}{|\alpha|}\right)^n \exp\left(-\frac{|\alpha|^2}{2}\right) \left(\frac{n}{|\alpha|} - |\alpha| - \frac{m-m_0}{\sigma}\right)^{-n}, & \text{for } \frac{m-m_0}{\sigma} \leq -\alpha. \end{cases}$$

describes the core of the resolution, while the second Gaussian function parametrizes the effect of the uncertainty in the primary vertex assignments.

Figures 1 and 2 show examples of fit projections onto the mass (left) and $\ell_{J/\psi}$ axes (right), for dimuons with $6.5 < p_T < 30\,\text{GeV}/c$ in two ranges of event centrality, 0-100% (top) and 0-10% (bottom), integrated over rapidity, $|y| < 2.4$ and for the forward region only, $1.6 < |y| < 2.4$. In the region $0.5 < \ell_{J/\psi} < 1\,\text{mm}$, the data are not well described by the fit. It has been found that this difference between the data and the fit is localized in the negative rapidity region of the detector, while the shape of the data in the positive rapidity region is well described by the fit. This is illustrated in Fig. 3. The measured b-fractions are $f_b = 0.235 \pm 0.008$ for $y < 0$ and $f_b = 0.234 \pm 0.009$ for $y > 0$ and agree within their statistical uncertainties. Such an agreement has been verified in all bins under consideration.

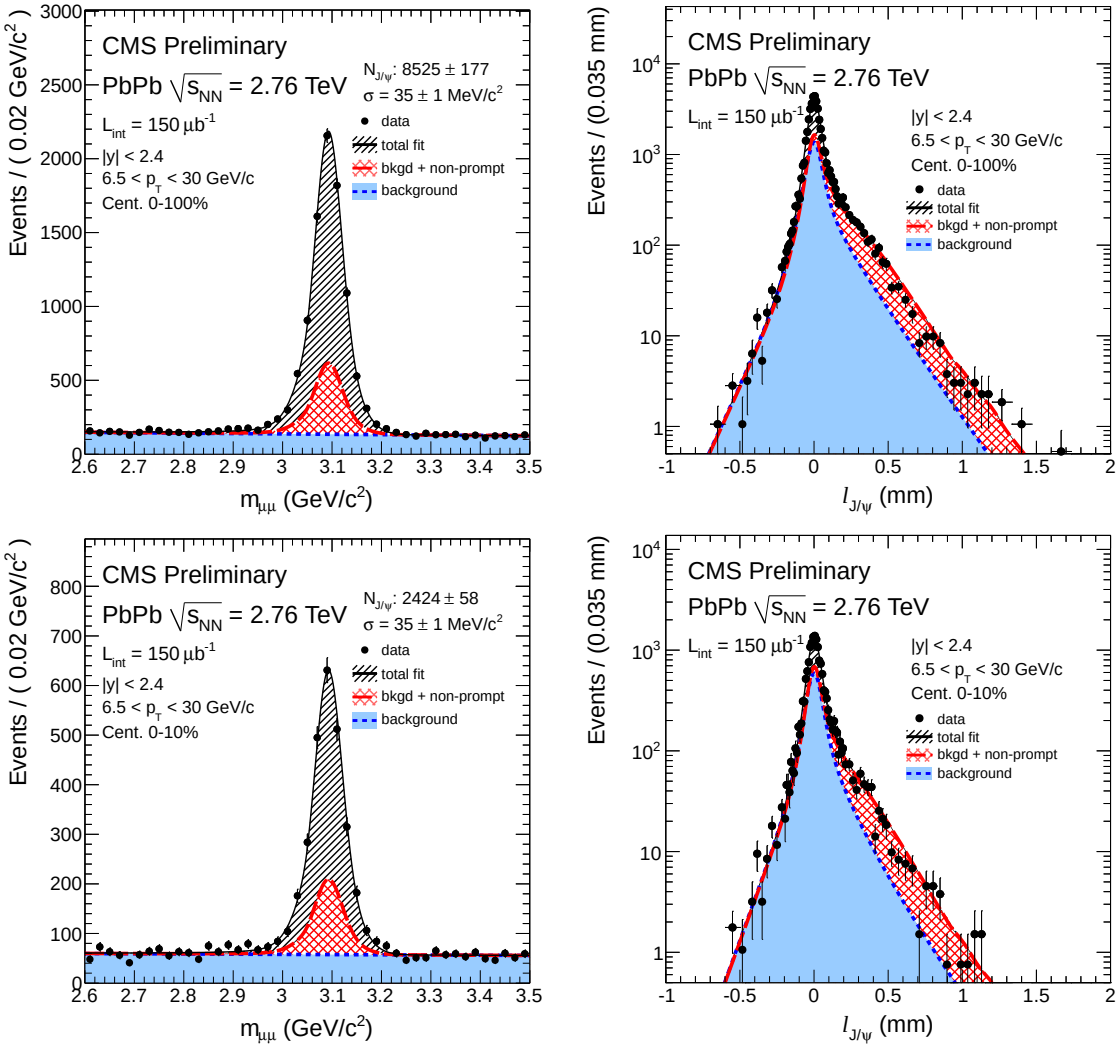

Figure 1: Invariant-mass spectra (left) and pseudo-proper decay length distribution (right) of $\mu^+\mu^-$ pairs integrated over centrality (top) and 0–10% most central collisions (bottom). The spectra are integrated over the rapidity range $0 < |y| < 2.4$ and the p_T range $6.5 < p_T < 30\,\text{GeV}/c$. The projections of the two-dimensional fit onto the respective axes are overlaid as solid black lines. The dashed red lines show the fitted contribution of non-prompt J/ψ. The fitted background contributions are shown as dotted blue lines.

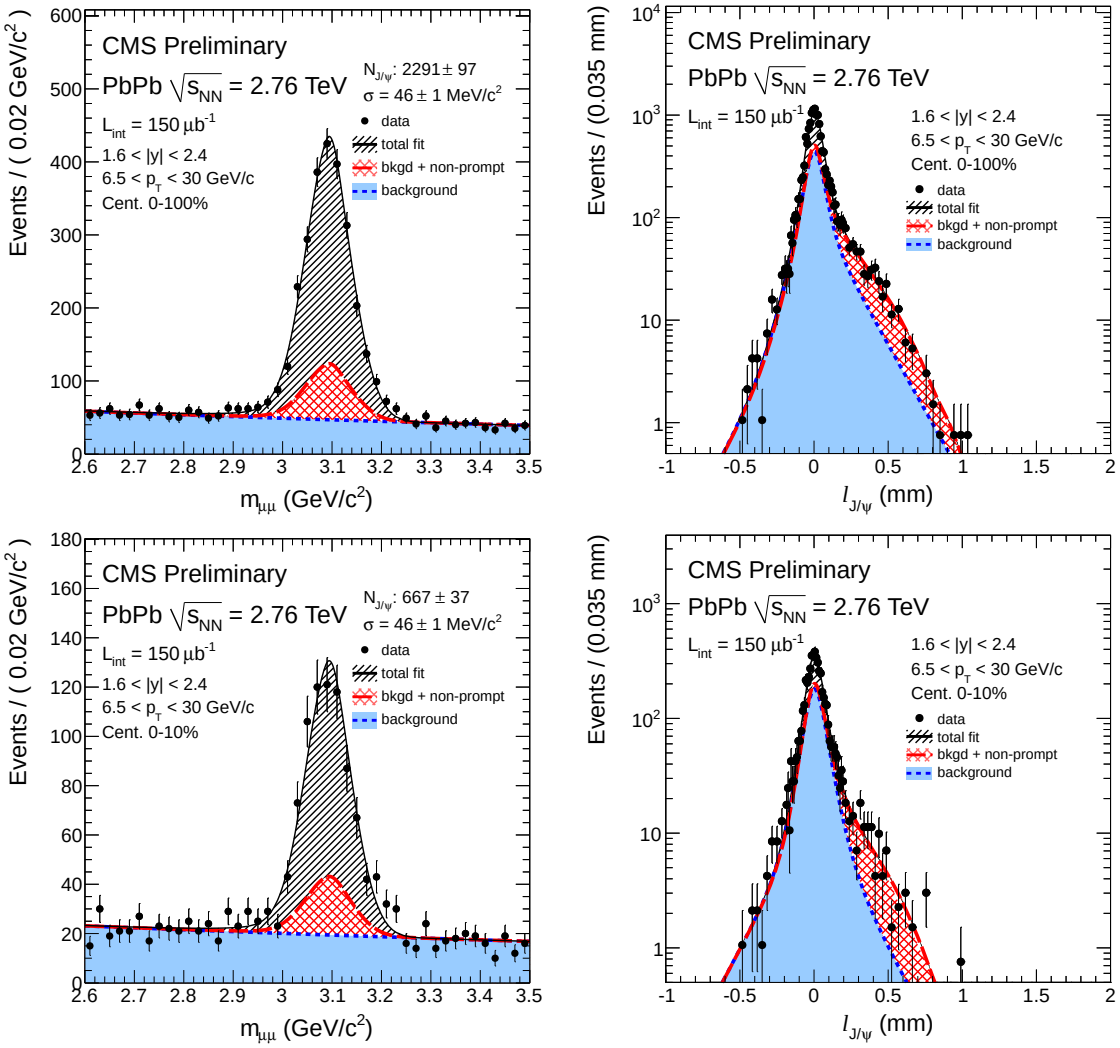

Figure 2: Invariant-mass spectra (left) and pseudo-proper decay length distribution (right) of $\mu^+\mu^-$ pairs integrated over centrality (top) and 0–10% most central collisions (bottom). The spectra are integrated over the rapidity range $1.6 < |y| < 2.4$ and the p_T range $6.5 < p_T < 30\,\mathrm{GeV}/c$. The projections of the two-dimensional fit onto the respective axes are overlaid as solid black lines. The dashed red lines show the fitted contribution of non-prompt J/ψ. The fitted background contributions are shown as dotted blue lines.

Several sources of systematic uncertainties have been considered, using the same procedures as in ref. [18]. Alternative shapes and methods have been used to fit mass and lifetime distributions. A Crystal Ball function is used for dimuon mass signal shape, and a straight line is used for dimuon mass background. For the signal parameters that are fixed to the 0–100% in differential centrality bins, an uncertainty is calculated by performing constrained fits in which the "constrained" parameters are allowed to vary with a Gaussian probability density function. The mean of the constraining Gaussian and the initial value of the constrained parameters come from the fitting in 0–100% bin with no fixed parameters. The error of the parameters in 0–100% bin is used as a width of the constraining Gaussian. With the constrained fitting method, all uncertainties from fixed parameters are determined.

For the lifetime fits, the case of only one Gaussian for the resolution function is considered, to

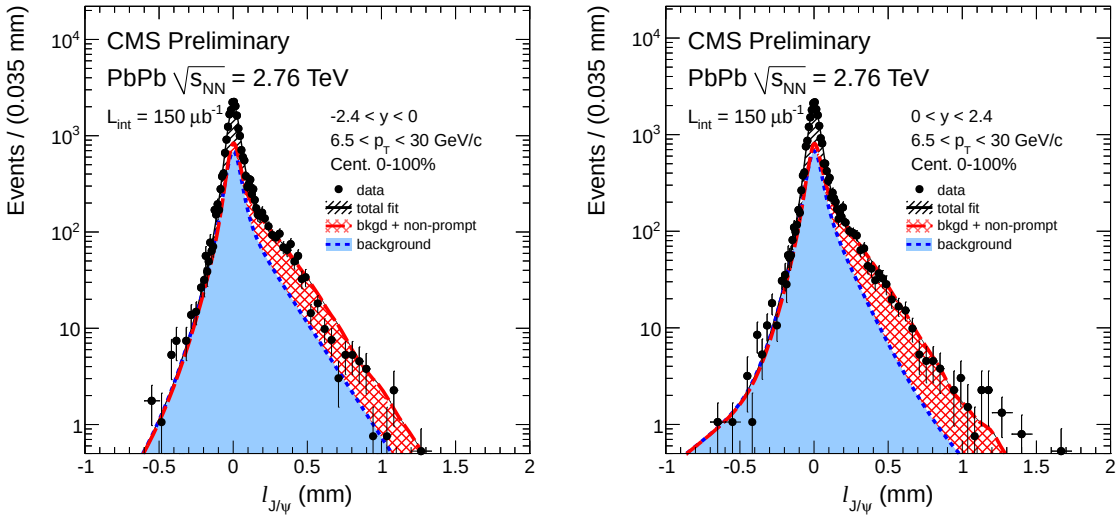

Figure 3: Pseudo-proper decay length distribution of $\mu^+\mu^-$ pairs with $y < 0$ (left) and $y > 0$ (right) integrated over centrality. The spectra are integrated over the p_T range $6.5 < p_T < 30\,\text{GeV}/c$. The projections of the two-dimensional fit onto the respective axes are overlaid as solid black lines. The dashed red lines show the fitted contribution of non-prompt J/ψ. The fitted background contributions are shown as dotted blue lines.

determine the effect of the tail components. Resolution function parameters determined from data are used to assess the uncertainty due to any possible difference between the MC template and data.

The systematic uncertainties from the yields extraction vary between 0.2 % and 1.7% for the prompt J/ψ yield, while the non-prompt J/ψ yield has uncertainties up to 4.5%.

For the pp data sample, no modification to the default fitting method compared to the one described in [18] was made. The systematic uncertainties do include though the differences obtained when fitting with the same method as the PbPb sample (the per-event-error consideration).

5 Efficiency

The trigger, reconstruction, and selection efficiencies of $\mu^+\mu^-$ pairs are evaluated using simulated Monte Carlo (MC) signal events embedded in simulated PbPb events, following the same procedure as for the 2010 PbPb results [18]. The individual components of the MC efficiency are cross-checked using muons from J/ψ decays in simulated and collision data with a technique called *tag-and-probe* (T&P), as described in [18].

The only difference compared to the 2010 analysis consists in using the trigger results from the data-driven T&P to correct the MC efficiencies used for the final results. Figure 4 shows the T&P single muon efficiencies versus centrality, pseudo-rapidity and muon p_T. The 'tags' in this case are muons that pass all acceptance and quality cuts used in the analysis and are matched to a single muon trigger. The 'probe' is a similar muon, but with no specific trigger matching requirement. The 'passing probes' are matched (in η and ϕ) to the dimuon trigger used for the analysis. The correction is parametrized by the ratio of a fit to the MC and to the real data single muon efficiencies obtained with T&P, and it is applied as a weight for each dimuon, according to the p_T of the single muons. A global uncertainty of 10% was assigned due to the

weighting, and calculated as twice (for the two muons) the difference between the minimum bias efficiencies in the two cases (in legend of Figure 4).

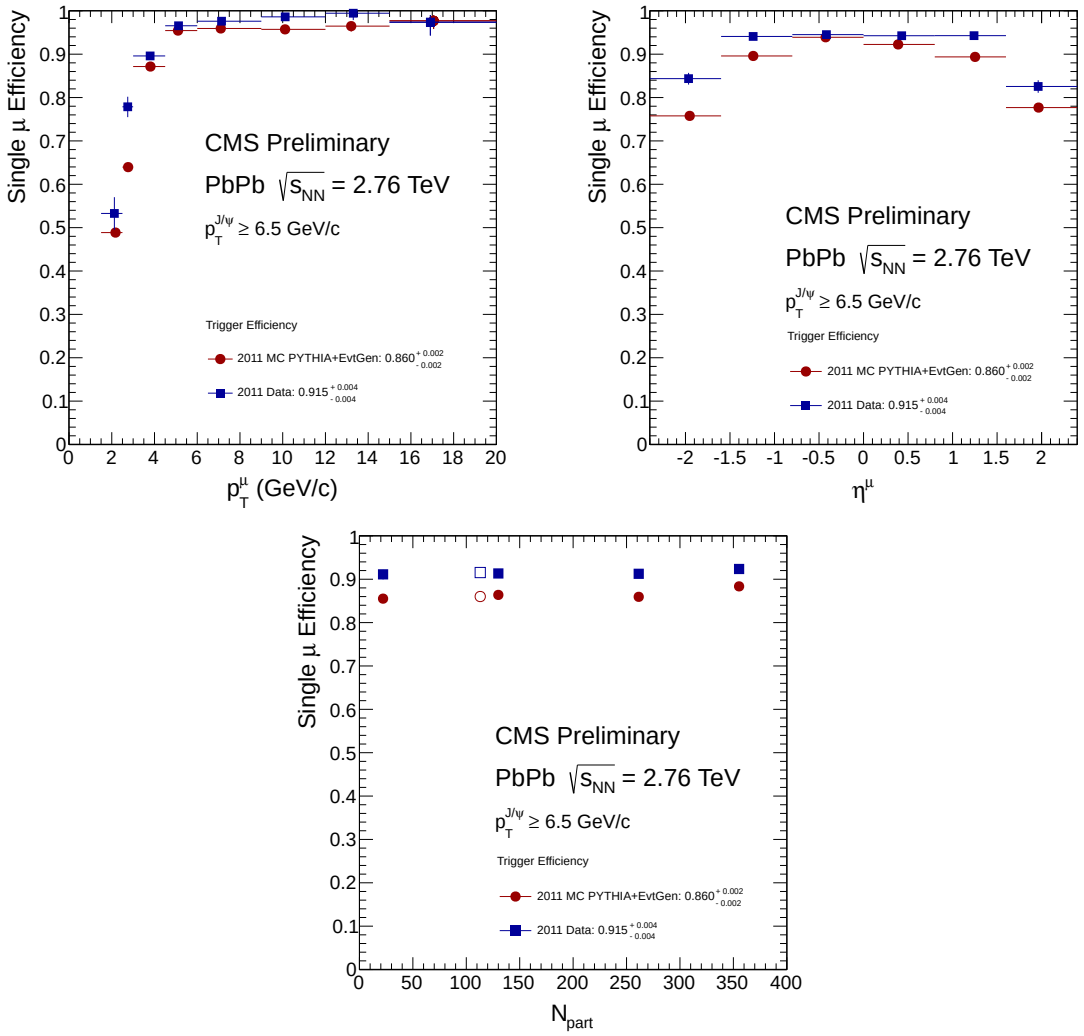

Figure 4: Comparison of the trigger efficiency measured with T&P in data (blue squares) and MC (red circles) as function of p_T (top left), η (top right) and centrality (bottom). The open symbols represent the minbias points.

From the T&P results a 16% systematic uncertainty on muon identification and tracking reconstruction efficiencies of the muon pair is assigned. This represents, added in quadrature, the largest data-MC single muon efficiency difference, among the centrality bins, for the muon identification, and the difference in the most peripheral bin for the tracking efficiency. These choices were made considering the regions where the background level allowed a good fit of all mass distributions involved in the T&P method. The ratio of the efficiencies in PbPb and pp is used in the R_{AA} calculation. Considering that the tracking and all cuts were the same in the two analyses, in the final R_{AA} uncertainty, the T&P uncertainty on data-MC agreement is applied only for the multiplicity-dependent fraction of the two efficiencies and hence propagated like $16\% \times (1 - \epsilon_{\mathrm{PbPb}}/\epsilon_{\mathrm{pp}})$.

Different polarizations of the J/ψ can cause different single-muon angular distributions in the laboratory frame and, hence, different probabilities for the muons to fall inside the CMS detec-

tor acceptance. If, due to physics, the polarizations were different in pp and PbPb, the effect would not cancel in the R_{AA} ratio. Since the quarkonium polarization has not been measured in heavy-ion or pp collisions at $\sqrt{s_{\rm NN}}$ = 2.76 TeV, the prompt J/ψ results are quoted for the unpolarized scenario only. We note, however, that the only existing measurement, published by the ALICE collaboration, for inclusive J/ψ in pp collisions at $\sqrt{s_{\rm NN}}$ = 7 TeV, [29], shows a polarization which is consistent with zero. For non-prompt J/ψ the results are reported for the polarization predicted by EVTGEN [2]. No systematic uncertainties due to polarization effects are assigned to the final results.

6 Systematic uncertainties

The total systematic uncertainty on the R_{AA} is estimated by summing in quadrature the different contributions. The ranges of the variations are summarized in Table 1. The yield extraction uncertainties increase from mid- to forward-rapidity, and for PbPb also from central to peripheral bins. The uncertainties associated with muon reconstruction have a smooth increase from peripheral to central bins, mapping the centrality dependence of efficiency in PbPb, which is smaller in central events compared to peripheral events. The T_{AA} uncertainties increase from central to peripheral bins.

Table 1: Systematic uncertainties on the prompt and non-prompt J/ψ R_{AA} measured in PbPb collisions.

	prompt J/ψ (%)	non-prompt J/ψ (%)
PbPb yield extraction	0.2–1.7	0.6–4.5
pp yield extraction	0.3–1.6	1.7–8.4
T&P^{recoValidation} $\times$ $(1 - \epsilon_{\rm PbPb}/\epsilon_{\rm pp})$	1–9	1–10
T&P^{triggerCorrection}	10	10
T_{AA}	4.1–18	4.3–15
Total	10.8–23	11.1–22.7

In all the results shown in Figs. 5- 8, statistical uncertainties will be represented by error bars and systematic uncertainties by boxes on the points. Boxes plotted at $R_{AA} = 1$ indicate the scale of the global uncertainties.

For results plotted as a function of $p_{\rm T}$ or rapidity: a) the statistical and systematic uncertainties include, added in quadrature, the statistical and systematical uncertainties from both PbPb and pp samples; b) the systematic uncertainty on T_{AA}, as well as the pp luminosity uncertainty, enter as a global uncertainty; they are added in quadrature and plotted as a gray box as a scale uncertainty at $R_{AA} = 1$. As a function of centrality: a) the statistical and systematic uncertainties from pp are added in quadrature together with the pp luminosity uncertainty, and plotted as a colored box, as a scale uncertainty, at $R_{AA} = 1$; b) the uncertainty on T_{AA} varies point-to-point and is included in the systematic uncertainties.

[2] The effective polarization in EVTGEN is roughly $\lambda_\theta = -0.4$. However this is not a well-defined value, but just the sum of many $B \to {\rm J}/\psi X$ modes in which the spin alignment is either forced by angular momentum conservation or given as input from measured values of helicity amplitudes in decays.

7 Results

7.1 Prompt J/ψ

In Fig. 5 the R_{AA} of high-p_{T} prompt J/ψ as function of centrality, p_{T} and rapidity is shown, integrating in each case over the other two variables. No p_{T} dependence is observed while the rapidity dependence is very weak, consistent with being at the same level of suppression. A slow decrease of the suppression *vs.* the event centrality is observed, with R_{AA} being still suppressed in the most peripheral bin in which the measurement was performed (60–100%). The centrality-integrated R_{AA} value measured for $6.5 < p_{\mathrm{T}} < 30\,\mathrm{GeV}/c$ and $|y| < 2.4$ is $0.34 \pm 0.02\,(\mathrm{stat.}) \pm 0.04\,(\mathrm{syst.})$.

A double-differential study is possible with 2011 data, in which a simultaneous binning in centrality and rapidity, or in centrality and p_{T} is done. Figure 6 left shows the R_{AA} rapidity dependence of high-p_{T} ($6.5 < p_{\mathrm{T}} < 30\,\mathrm{GeV}/c$) prompt J/$\psi$. The same centrality dependence is observed, independent of rapidity. Figure 6 right shows the p_{T} dependence in the forward rapidity ($1.6 < |y| < 2.4$), where CMS has dimuon acceptance down to $p_{\mathrm{T}} = 3\,\mathrm{GeV}/c$. The low-$p_{\mathrm{T}}$ J/ψ are consistent with the suppression of the high-p_{T} prompt J/ψ over all centrality bins.

7.2 Non-prompt J/ψ

In Fig. 7 the R_{AA} of high-p_{T} non-prompt J/ψ as function of centrality, p_{T} and rapidity are shown, integrating in each case over the other two variables. A hint of an increase of the suppression with increasing p_{T} and rapidity can be noted. A slow increase of the suppression is observed with increasing centrality of the collision. The centrality-integrated R_{AA} value measured for $6.5 < p_{\mathrm{T}} < 30\,\mathrm{GeV}/c$ and $|y| < 2.4$ is $0.45 \pm 0.05\,(\mathrm{stat.}) \pm 0.06\,(\mathrm{syst.})$.

As for the prompt case, a double differential study is possible with 2011 data, simultaneously binning in centrality and rapidity or p_{T}. Figure 8 left shows, in bins of centrality, the R_{AA} rapidity dependence of high-p_{T} ($6.5 < p_{\mathrm{T}} < 30\,\mathrm{GeV}/c$) non-prompt J/$\psi$. Figure 8 right shows also versus centrality, the p_{T} dependence in the forward rapidity ($1.6 < |y| < 2.4$) for low, $3 < p_{\mathrm{T}} < 6.5\,\mathrm{GeV}/c$ and high-p_{T}, $6.5 < p_{\mathrm{T}} < 30\,\mathrm{GeV}/c$, non-prompt J/$\psi$.

For high-p_{T} non-prompt J/ψ there is an indication of less suppression in the mid-rapidity region compared to the forward region, while the p_{T} dependence results show hints of less suppression at low-p_{T}. However, in both cases, within the present uncertainties, all measured values are compatible with being the same.

8 Summary

The prompt and non-prompt J/ψ production have been measured separately in the $150\,\mu\mathrm{b}^{-1}$ data recorded during the PbPb collisions in November 2011. The 20-fold increase in data volume compared to the 2010 PbPb run allowed for detailed and more differential measurements. Finer bins in centrality and p_{T}, and centrality and rapidity or centrality and p_{T} simultaneous binning were possible.

The prompt J/ψ, integrated over the rapidity range $|y| < 2.4$ and high-p_{T}, $6.5 < p_{\mathrm{T}} < 30\,\mathrm{GeV}/c$, has been measured in 12 centrality bins, starting with the 0-5% bin (most central), up to to 60–100% bin (most peripheral). The R_{AA} shows a steady and smooth decrease of suppression with the R_{AA} remaining < 1 in the most peripheral bin. Integrated over rapidity and centrality, there is no evidence of suppression dependence with p_{T}, confirming the 2010 results published

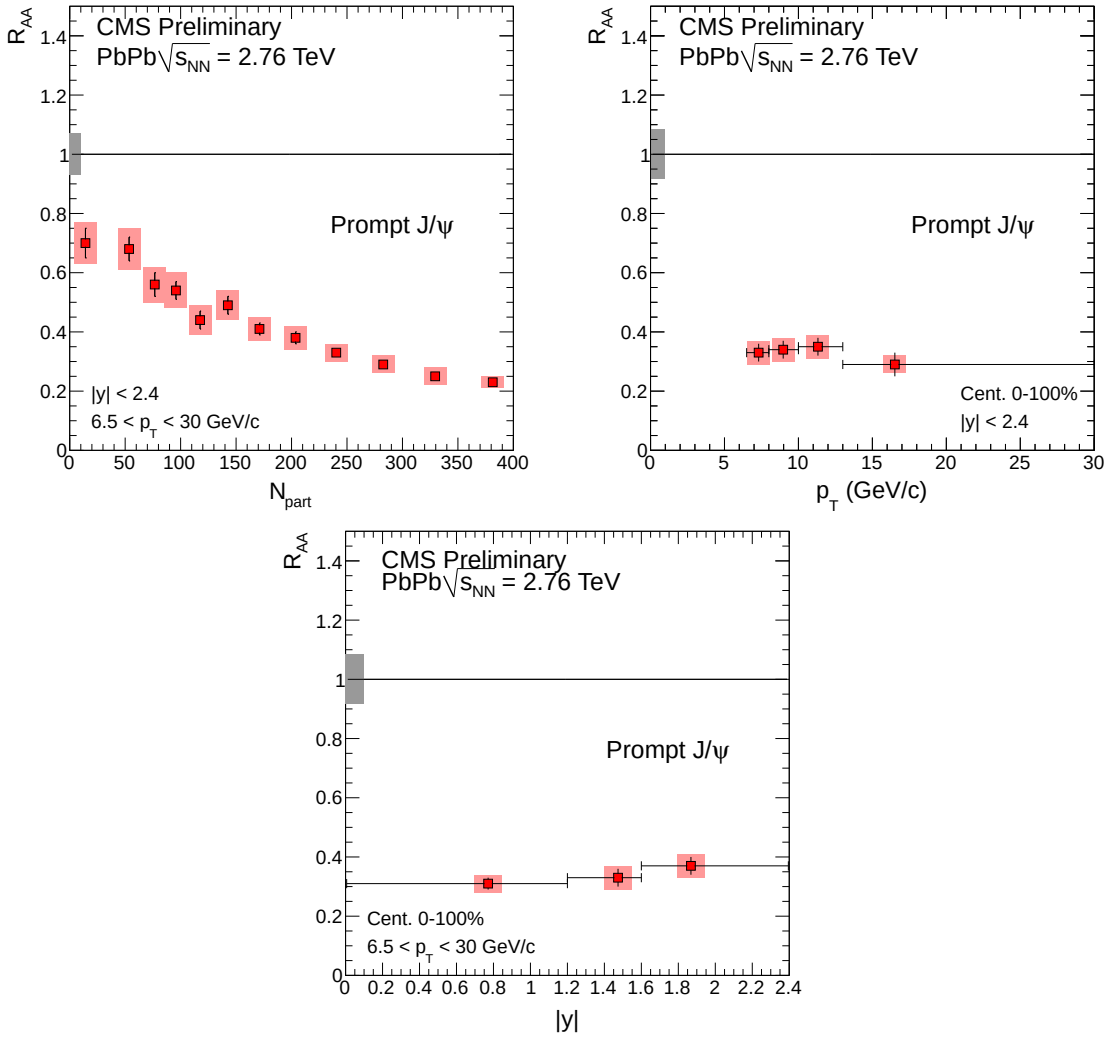

Figure 5: The nuclear modification factor as function of centrality *(left)*, p_{T} *(right)* and rapidity *(bottom)* for the prompt J/ψ. The gray boxes plotted at R_{AA} =1 indicate the scale of the global uncertainties: (left) the uncertainty of 6% on the measured integrated luminosity of the pp data sample, together with the statistical and systematic uncertainty on the pp data set; (right and bottom) the pp luminosity and the T_{AA} uncertainties. The bin boundaries are indicated by small horizontal lines where meaningful.

in two bins. There is no significant rapidity dependence of the high-p_{T} prompt J/ψ R_{AA} when integrating over centrality and p_{T}. The low-p_{T} prompt J/ψ are consistent with the suppression of the high-p_{T} prompt J/ψ over all centrality bins. This is different than the preliminary ψ(2S) measurement by CMS [30], that shows an opposite trend of the low-p_{T} and high-p_{T} R_{AA} dependence, albeit, in slightly different rapidity kinematic regions.

The non-prompt J/ψ rapidity, p_{T} and fine centrality-differential measurements are novel in all aspects. The centrality dependence shows a slow decrease of the R_{AA} with decreasing centrality. For high-p_{T} non-prompt J/ψ there is an indication of less suppression in the mid-rapidity region compared to forward region, while the p_{T} dependence results show hints of less suppression at low p_{T}. However, in both cases, within the present uncertainties, all measured values are compatible with being the same. These measurements represent the first unambiguous and detailed look at the b-quark energy loss dependence on centrality, p_{T} and rapidity.

In conclusion, CMS presents novel measurements in two fundamental channels for the study of high-density QCD medium created in central heavy-ion collisions: charmonium production, via prompt J/ψ, and b-quark energy loss, via non-prompt J/ψ from B-hadron decays, measured over a large kinematic range. They represent updates of the 2010 analysis, with single and double differential new results.

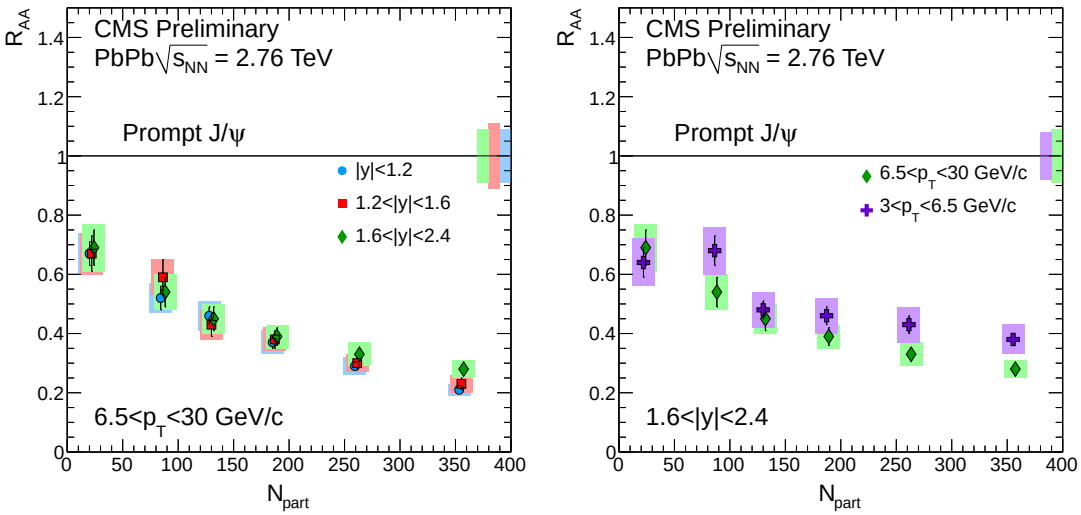

Figure 6: Left: R_{AA} as function of centrality, for the high-p_{T} prompt J/ψ, $6.5 < p_{\mathrm{T}} < 30\,\mathrm{GeV}/c$, for three different rapidity regions. Right: R_{AA} as function of centrality, for the forward produced produced J/ψ, $1.6 < |y| < 2.4$, for two different p_{T} regions. The colored boxes plotted at R_{AA} =1 indicate the scale of the global uncertainties: the uncertainty of 6% on the measured integrated luminosity of the pp data sample, together with the statistical and systematic uncertainty corresponding to each pp data set. The high-p_{T} mid- and forward-rapidity points are shifted horizontally by $\Delta N_{\mathrm{part}} = 2$ for better visibility.

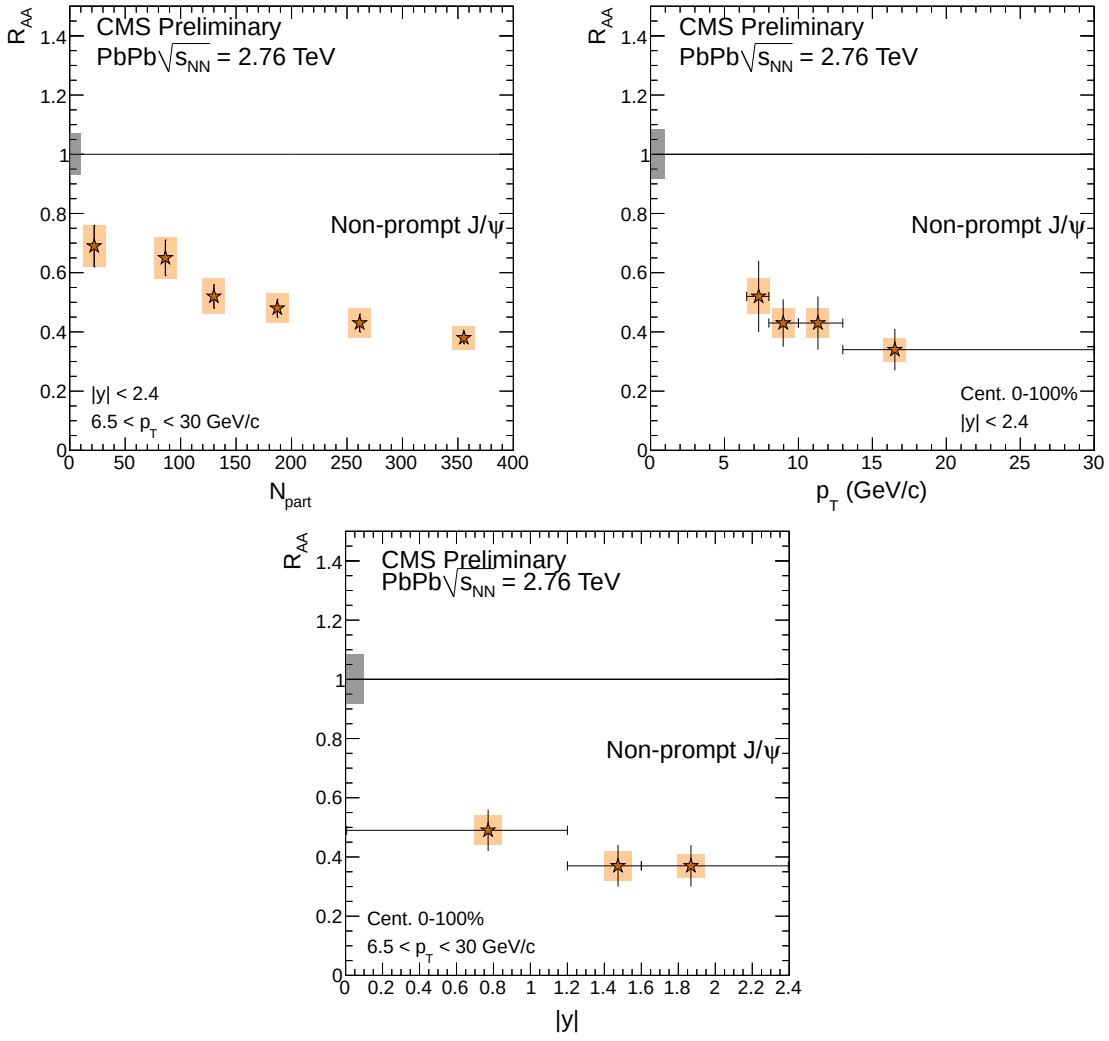

Figure 7: The nuclear modification factor as function of centrality *(left)*, p_{T} *(right)* and rapidity *(bottom)* for the non-prompt J/ψ. The gray boxes plotted at R_{AA} =1 indicate the scale of the global uncertainties: (left) the uncertainty of 6% on the measured integrated luminosity of the pp data sample, together with the statistical and systematic uncertainty on the pp data set; (right and bottom) the pp luminosity and the T_{AA} uncertainties. The bin boundaries are indicated by small horizontal lines where meaningful.

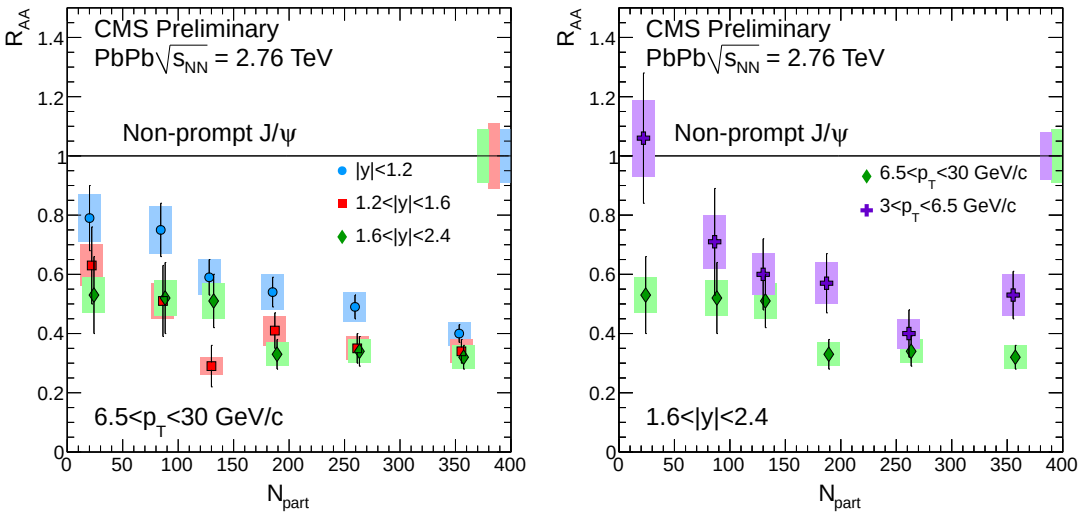

Figure 8: Left: R_{AA} as function of centrality, for the high-p_{T} non-prompt J/ψ, $6.5 < p_{\mathrm{T}} < 30\,\mathrm{GeV}/c$, for three different rapidity regions. Right: R_{AA} as function of centrality, for the forward produced non-prompt J/ψ, $1.6 < |y| < 2.4$, for two different p_{T} regions. The colored boxes plotted at R_{AA} =1 indicate the scale of the global uncertainties: the uncertainty of 6% on the measured integrated luminosity of the pp data sample, together with the statistical and systematic uncertainty corresponding to each pp data set. The high-p_{T} mid- and forward-rapidity points are shifted horizontally by $\Delta N_{\mathrm{part}} = 2$ for better visibility.

References

[1] F. Karsch and E. Laermann, "Thermodynamics and in-medium hadron properties from lattice QCD", in *Quark-Gluon Plasma III*, R. C. Hwa and X.-N. Wang, eds. World Scientific Publishing Co. Pte. Ltd., 2004. arXiv:hep-lat/0305025.

[2] E. V. Shuryak, "Theory of Hadronic Plasma", *Sov. Phys. JETP* **47** (1978) 212.

[3] T. Matsui and H. Satz, "J/ψ suppression by quark-gluon plasma formation", *Phys. Lett. B* **178** (1986) 416, doi:10.1016/0370-2693(86)91404-8.

[4] R. Vogt, "Cold Nuclear Matter Effects on J/ψ and Y Production at energies available at the CERN Large Hadron Collider (LHC)", *Phys. Rev. C* **81** (2010) 044903, doi:10.1103/PhysRevC.81.044903, arXiv:1003.3497.

[5] X. Zhao and R. Rapp, "Medium modifications and production of charmonia at LHC", *Nucl. Phys. A* **859** (2011) 114, doi:10.1016/j.nuclphysa.2011.05.001, arXiv:1102.2194.

[6] X. Zhao and R. Rapp, "Charmonium in medium: From correlators to experiment", *Phys. Rev. C* **82** (2010) 064905, doi:10.1103/PhysRevC.82.064905, arXiv:1008.5328.

[7] A. Andronic, P. Braun-Munzinger, K. Redlich et al., "Statistical hadronization of heavy quarks in ultra-relativistic nucleus–nucleus collisions", *Nucl. Phys. A* **789** (2007) 334, doi:10.1016/j.nuclphysa.2007.02.013, arXiv:nucl-th/0611023.

[8] A. Capella, L. Bravina, E. Ferreiro et al., "Charmonium dissociation and recombination at RHIC and LHC", *Eur. Phys. J. C* **58** (2008) 437, doi:10.1140/epjc/s10052-008-0772-6, arXiv:0712.4331.

[9] R. L. Thews and M. L. Mangano, "Momentum spectra of charmonium produced in a quark-gluon plasma", *Phys. Rev. C* **73** (2006) 014904, doi:10.1103/PhysRevC.73.014904, arXiv:nucl-th/0505055.

[10] L. Yan, P. Zhuang, and N. Xu, "J/ψ production in quark-gluon plasma", *Phys. Rev. Lett.* **97** (2006) 232301, doi:10.1103/PhysRevLett.97.232301, arXiv:nucl-th/0608010.

[11] L. Grandchamp, S. Lumpkins, D. Sun et al., "Bottomonium production at $\sqrt{s_{\rm NN}} = 200$ GeV and $\sqrt{s_{\rm NN}} = 5.5$ TeV", *Phys. Rev. C* **73** (2006) 064906, doi:10.1103/PhysRevC.73.064906, arXiv:hep-ph/0507314.

[12] LHCb Collaboration, "Measurement of J/ψ production in pp collisions at $\sqrt{s} = 7$ TeV", *Eur. Phys. J. C* **71** (2011) 1645, doi:10.1140/epjc/s10052-011-1645-y, arXiv:1103.0423.

[13] CMS Collaboration, "Prompt and non-prompt J/ψ production in pp collisions at $\sqrt{s} = 7$ TeV", *Eur. Phys. J. C* **71** (2011) 1575, doi:10.1140/epjc/s10052-011-1575-8, arXiv:1011.4193.

[14] ATLAS Collaboration, "Measurement of the differential cross-sections of inclusive, prompt and non-prompt J/ψ production in pp collisions at $\sqrt{s} = 7$ TeV", *Nucl. Phys. B* **850** (2011) 387, doi:10.1016/j.nuclphysb.2011.05.015, arXiv:1104.3038.

[15] Y. L. Dokshitzer and D. Kharzeev, "Heavy quark colorimetry of QCD matter", *Phys. Lett. B* **519** (2001) 199, doi:10.1016/S0370-2693(01)01130-3, arXiv:hep-ph/0106202.

[16] N. Armesto, A. Dainese, C. A. Salgado et al., "Testing the color charge and mass dependence of parton energy loss with heavy-to-light ratios at BNL RHIC and CERN LHC", *Phys. Rev. D* **71** (2005) 054027, doi:10.1103/PhysRevD.71.054027, arXiv:hep-ph/0501225.

[17] S. Peigne and A. Peshier, "Collisional energy loss of a fast heavy quark in a quark-gluon plasma", *Phys. Rev. D* **77** (2008) 114017, doi:10.1103/PhysRevD.77.114017, arXiv:0802.4364.

[18] CMS Collaboration, "Suppression of non-prompt J/psi, prompt J/psi, and Y(1S) in PbPb collisions at $\sqrt{s_{\mathrm{NN}}}$ = 2.76 TeV", arXiv:1201.5069.

[19] ALICE Collaboration, "J/ψ production at low transverse momentum in PbPb collisions at $\sqrt{s_{\mathrm{NN}}}$ = 2.76 TeV", arXiv:1202.1383. submitted to Phys. Rev. Lett.

[20] M. L. Miller, K. Reygers, S. J. Sanders et al., "Glauber modeling in high-energy nuclear collisions", *Ann. Rev. Nucl. Part. Sci.* **57** (2007) 205, doi:10.1146/annurev.nucl.57.090506.123020, arXiv:nucl-ex/0701025.

[21] CMS Collaboration, "The CMS experiment at the CERN LHC", *JINST* **3** (2008) S08004, doi:10.1088/1748-0221/3/08/S08004.

[22] CMS Collaboration, "Measurement of momentum scale and resolution using low-mass resonances and cosmic ray muons", CMS Physics Analysis Summary TRK-2010/004, (2010).

[23] CMS Collaboration, "Observation and studies of jet quenching in PbPb collisions at $\sqrt{s_{\mathrm{NN}}}$ = 2.76 TeV", *Phys. Rev. C* **84** (2011) 024906, doi:10.1103/PhysRevC.84.024906, arXiv:1102.1957.

[24] CMS Collaboration, "CMS physics technical design report: Addendum on high density QCD with heavy ions", *J. Phys. G* **34** (2007) 2307, doi:10.1088/0954-3899/34/11/008.

[25] C. Roland (on behalf of the CMS Collaboration), "Track reconstruction in heavy ion collisions with the CMS silicon tracker", *Nucl. Instrum. Meth. A* **566** (2006) 123, doi:10.1016/j.nima.2006.05.023.

[26] ALEPH Collaboration, "Measurement of the $\overline{\mathrm{B}}^0$ and B^- meson lifetimes", *Phys. Lett. B* **307** (1993) 194, doi:10.1016/0370-2693(93)90211-Y.

[27] ALEPH Collaboration, "Errata: Measurement of the $\overline{\mathrm{B}}^0$ and B^- meson lifetimes", *Phys. Lett. B* **325** (1994) 537, doi:10.1016/0370-2693(94)90054-X.

[28] CMS Collaboration Collaboration, "J/ψ and ψ(2S) production in pp collisions at $\sqrt{s}$ = 7 TeV", *JHEP* **02** (2012) arXiv:1111.1557.

[29] ALICE Collaboration, "J/ψ polarization in pp collisions at $\sqrt{s}$ = 7 TeV", arXiv:1111.1630. submitted to Phys. Rev. Lett.

[30] CMS Collaboration, "Measurement of the ψ(2S) meson in PbPb collisions at $\sqrt{s_{\mathrm{NN}}}$ 2.76 TeV", CMS Physics Analysis Summary HIN-2012/008, (2012).